



Detection of fluid flow variations at the Nankai Trough by electric and magnetic measurements in boreholes or at the seafloor

Laurence Jouniaux, Jean-Pierre Pozzi, Jean Berthier, Philippe Massé

► To cite this version:

Laurence Jouniaux, Jean-Pierre Pozzi, Jean Berthier, Philippe Massé. Detection of fluid flow variations at the Nankai Trough by electric and magnetic measurements in boreholes or at the seafloor. *Journal of Geophysical Research: Solid Earth*, 1999, 104,B12 (B12), pp.29293-29309. 10.1029/1999JB900102 . hal-00108292

HAL Id: hal-00108292

<https://hal.science/hal-00108292>

Submitted on 25 Jan 2021

HAL is a multi-disciplinary open access archive for the deposit and dissemination of scientific research documents, whether they are published or not. The documents may come from teaching and research institutions in France or abroad, or from public or private research centers.

L'archive ouverte pluridisciplinaire **HAL**, est destinée au dépôt et à la diffusion de documents scientifiques de niveau recherche, publiés ou non, émanant des établissements d'enseignement et de recherche français ou étrangers, des laboratoires publics ou privés.

Detection of fluid flow variations at the Nankai Trough by electric and magnetic measurements in boreholes or at the seafloor

Laurence Jouniaux and Jean-Pierre Pozzi

École Normale Supérieure, Laboratoire de Géologie, UMR 8538, Paris, France

Jean Berthier and Philippe Massé

Laboratoire d'électronique, technologies et instrumentations, CEA, Grenoble, France

Abstract. Detection of changes in the flow rate of expelled fluids in accretionary prisms by monitoring of electric and magnetic fields is discussed. A numerical model of the electric and magnetic fields associated with fluid flow variations at the Nankai Trough is presented which gives a numerical solution of the coupled system of electric convection currents and conduction currents that directly determines the magnetic anomaly itself. Measurements in a borehole located between two vents are shown to be well adapted to detection of fluid flow variations using the vertical gradient of the electric potential and the horizontal magnetic field. The vertical electric field is about 10 mV/km up to 500 m depth where there is a lithologic reflector and about 50 mV/km below this reflector. The horizontal gradient of the magnetic field is 2 nT/km at the seafloor. Modelization with a lower fault conductivity and a larger décollement thickness has also been modeled. The vertical gradient of the horizontal magnetic field is ~5 to 15 nT/km. A variation of 3 mV and 1.5 to 3 nT at 600 m depth in a borehole could reveal a fluid flow rate variation of 20%, which is a reasonable fluid flow change based on some observations at short-scale time. Since a 1.5 to 3 nT anomaly seems easier to detect than a 3 mV anomaly, it is likely that the variation of the magnetic field would more sensitively reveal fluid flow variations. When monitoring the magnetic field at the seafloor, a change of 0.4 nT/km in the horizontal gradient could reveal a fluid flow rate variation of 20%.

1. Introduction

Accretionary prisms develop at some convergent margins from material offscraped at the deformation front. Accretionary prisms are composed of saturated sediments. As sediments deform, fluid pressure rises, and fluid is expelled both through tectonically induced consolidation and thermally induced dehydration processes. The décollement zone, essentially the plate boundary, separates the undeformed underthrust sediments from a complexly deformed accretionary prism. Fluid flow out of accretionary prisms occurs by distributed flow through intergranular permeability and by focused flow along fault zones and depends on large-scale permeability.

Elevated pore fluid pressure [Westbrook *et al.*, 1982] has long been recognized to maintain large parts of accretionary prisms near failure conditions [von Huene and Lee, 1982], resulting in complex interactions of strain regimes and fluid circulation. Expelled fluids from accretionary wedges have been shown to be transported from great depth within the prism [Cloos, 1984; Moore *et al.*, 1987; Moore and Vrolijk, 1992]. Changes of flow rate of expelled fluid could be related to the state of stress

[Moore, 1989; Vrolijk, 1987; Moore *et al.*, 1988] and to seismic hazard by the seismic pumping mechanism [Sibson *et al.*, 1975]. Studies along the outer eastern Nankai accretionary wedge showed that the fluid circulation is mostly related to active faults and near-surface highly permeable zones [Le Pichon *et al.*, 1992].

The Nankai trench results from the subduction of the Philippine plate under Eurasia (Figure 1). The Kaiko-Nankai area has been studied through the Kaiko scientific project since 1984 [Le Pichon *et al.*, 1992]. Improvement in the detection of precursors of strong earthquakes in the Tokai area is of great importance as a magnitude 8 earthquake is expected in the eastern part of this area with an expected displacement on the fault about 4 m [Ishibashi, 1981]. Monitoring long-term variations of fluid flow at the toe of the east Nankai Trough has been proposed to improve the prediction of earthquakes in the region. Electrokinetic potentials on the ocean floor have been proposed to monitor long term variations of fluid flow thus giving way to a precursory electric signal [Boulègue *et al.*, 1985; Segawa and Toh, 1992; Heinson and Segawa, 1997].

In this paper a very simple analytic model is first considered, then a three-step finite element numerical calculation [Massé and Berthier, 1995] taking into account the convection current induced by electrokinetic phenomena and the conduction current (back current) is developed. We discuss the possibility of detecting the variations of flow rates of fluids expelled from an accretionary wedge by monitoring changes of the magnetic or electric field. In this paper we propose to model and to compare

the possibilities of measurements: vertical electric field and horizontal magnetic field measurements in borehole, horizontal electric field, and horizontal magnetic field measurements at the seafloor. In our model, hydraulic flow and electric current have been modeled to compute the magnetic and electric field induced by the coupling between the fluid flow and the electric current. The questions are as follows: (1) What are the calculated values of the electric and magnetic fields related to fluid circulation not only at the surface of the prism but also deep in the sediment? (2) What are the relative advantages of surface or borehole measurements? (3) What measurements or combination of measurements constitute the best experimental strategy to monitor fluid flow variations?

2. Electrokinetic Effect

When a fluid is flowing through porous sediments, a convection electric current is induced. The electric current density associated to this electrokinetic phenomenon is

$$J_{\text{conv}} = C_s \sigma_r \text{grad } P \quad (1)$$

where $\text{grad } P$ is the pressure gradient creating the fluid flow, σ_r is the electric conductivity of the formation, and C_s is the electrokinetic coupling coefficient (in V/Pa). The electrokinetic coupling coefficient is

$$C_s = \Delta V / \Delta P = (\epsilon \zeta) / (\eta \sigma_f) \quad (2)$$

where ζ is the zeta potential at the rock/fluid interface, and σ_f , ϵ , and η are the electric conductivity, the electric permittivity, and the shear viscosity of the circulating fluid, respectively. This expression is the Helmholtz-Smoluchowski equation, and it implies that the surface conductivity is small and negligible compared to the fluid conductivity σ_f [Dukhin and Derjaguin, 1974]. Note that the electric current is assumed to have the same path as the fluid flow in the porous medium. The electrokinetic coupling coefficient is positive or negative depending on the sign of zeta potential; it is negative for most rock. Electrokinetic phenomena are due to the existence of an electric double layer formed at the solid-liquid interface [Stern, 1924]. The double layer is made up of a layer of ions adsorbed on the surface of the matrix and of a diffuse mobile layer extending into the liquid phase. The zeta potential is the electric potential on the plane closest to the surface of the matrix on which fluid is in motion. In response to this convection current a conduction current or back current, governed by Ohm's law, is generated and the total electric current density J is related to the forces $\text{grad } V$ and $\text{grad } P$ by

$$J = J_{\text{conv}} + J_{\text{cond}} = C_s \sigma_r \text{grad } P - \sigma_r \text{grad } V \quad (3)$$

where V is the electric potential [Nourbehecht, 1963].

3. Models

3.1. Simple Analytical Model

We have first developed a simplified analytical model to estimate the maximum electric and magnetic fields that could be induced by fluid flow. The fluid paths in accretionary prisms are commonly thought to be confined in the décollement and in the major thrust faults [Moore, 1989]. We have considered a simple geometry of two fault planes in which fluid is assumed to flow. These thrusts have an electrokinetic coupling coefficient C_s and

an electric conductivity σ_r . The permeability inside these thrusts is assumed to be very high compared to the permeability of the sediments outside of these thrusts, so that the fluid flow mainly occurs in these thrusts. Note that this geometry of fluid paths can be seen at several space scales. We consider two extreme approaches, one where the total electric current density within the thrusts is assumed to be equal to the convection current J_{conv} and the other where the total electric current density within the thrusts is assumed to be zero.

3.1.1. Case of maximum electric current density in major thrusts. We consider first a case where the conduction current J_{cond} created in response to the convection current J_{conv} occurs mostly outside of the thrusts (Figure 2a). This configuration is possible if the electric conductivity outside of the thrusts is not very low compared to the one within the thrusts. Then the electric current density $J = J_{\text{conv}}$ inside the thrusts can produce a magnetic field

$$B_x = \mu_0 / 2J \Delta Z \quad (4)$$

with ΔZ the width of the fault [Durand, 1953]. The magnetic field B_x induced by the fluid flow within the thrust is perpendicular to the direction of the electric current density sheet. B_x is independent of the distance to the thrust, as shown in Figure 2a. The magnetic field is uniform above and below each thrust with a discontinuity through the thrust. B_1 and B_2 are the magnetic fields induced by thrusts 1 and 2, respectively. Above and below the thrusts the magnetic fields add themselves - $(B_1 + B_2)$ and $(B_1 - B_2)$, respectively. Between the two thrusts the magnetic field will be lower since B_2 is subtracted from B_1 . We assume here that the electric conduction current density J_{cond} outside of the thrusts induces a magnetic field that is equal to zero by symmetry. To have an idea of the order of the magnetic field that could be generated, let us calculate the electric current density J within the thrusts $J = J_{\text{conv}}$, defining the maximum total current density. Thus the magnetic field induced by this current density sheet is

$$B_x = \mu_0 / 2J_{\text{conv}} \Delta Z = \mu_0 / 2 C_s \sigma_r \text{grad } P \Delta Z \quad (4')$$

where $\text{grad } P$ is the pressure gradient within the thrusts. If $\text{grad } P = \Delta P / \Delta Y = 10$ MPa/km (hydrostatic pressure gradient ρg), $\sigma_r = 0.28$ S/m and $C_s = -4$ mV/MPa (see section 3.2.2 for the justification of these values), the magnitude of the electric current density is $J_{\text{conv}} = 0.011$ mA/m². If we consider a width of fault $\Delta Z = 10$ m (for example, the décollement), $\mu_0 / 2 = 2\pi \cdot 10^{-7}$, the magnetic field is $B_x = 0.07$ nT. Above and below the two thrusts we could thus detect 0.14 nT by measuring the magnetic field inside the borehole.

Segawa and Toh [1992] computed the electric field at the ocean bottom induced by the streaming current density confined in a thrust and showed that the electric field at the ocean bottom was proportional to the electric current density. They assumed an electric convection current density $J_{\text{conv}} = 1$ mA/m² and no conduction current, and computed an electric field of 0.075 mV/m at the seafloor just above the exit of the fluid flow (in P_0 , for example, in Figure 2a) and of the order of 1 μ V/m at a distance of a few tens of meters from the entrainment of the fluid. Note that with a value of $J_{\text{conv}} = 0.01$ mA/m² as we computed, the electric field at the seafloor computed by Segawa and Toh [1992] would be 2 orders of magnitude smaller, meaning 0.01 μ V/m.

3.1.2. Case of zero electric current density in major thrusts. We consider now that the conduction current created in

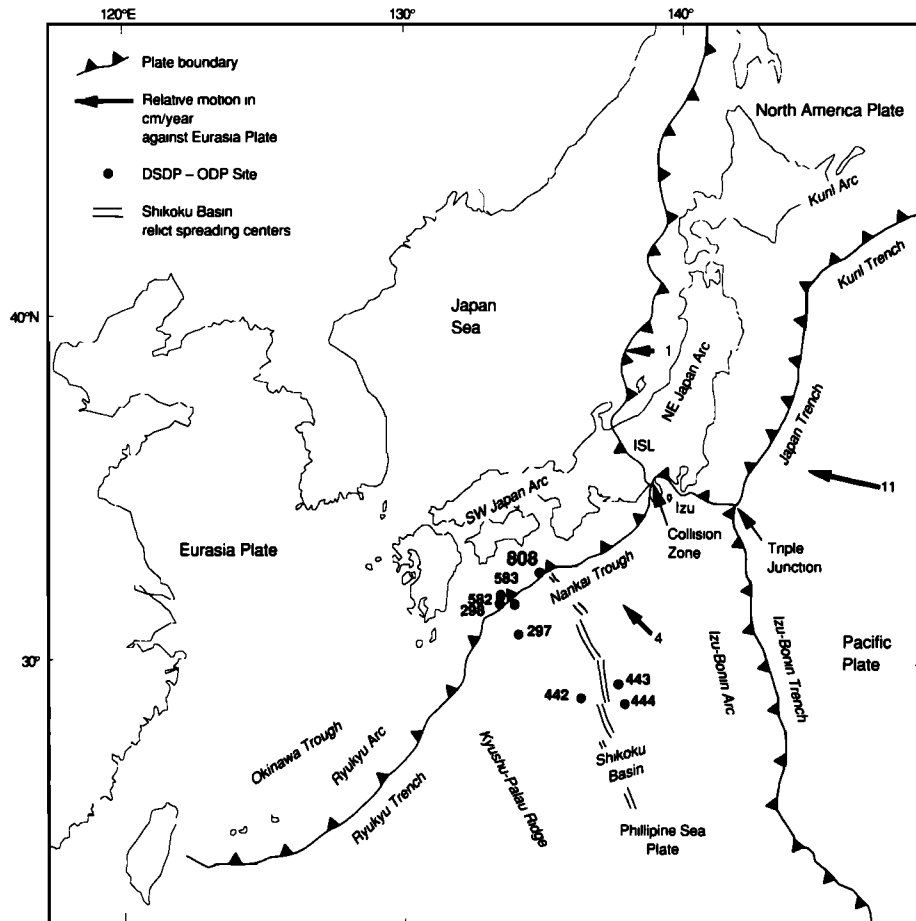


Figure 1. Location map, from Taira et al., 1991.

response to the convection current occurs mainly inside the thrusts (meaning that the electric conductivity inside the thrust is very high compared to the one in the adjacent sediments) and balances the convection current so that the total electric current density J is zero (Figure 2b). In this configuration, no magnetic field will be induced (equation (4)), and the electric field at the seafloor computed by Segawa and Toh [1992] would be zero, but the electric field within the thrusts will be maximum: $J = 0 = C_s \sigma_r \text{grad } P - \sigma_r \text{grad } V$ leads to $\text{grad } V = C_s \text{grad } P$. If we assume a hydrostatic pressure gradient in the thrust $\text{grad } P = 10 \text{ MPa/km}$ and an electrokinetic coupling coefficient $C_s = -4 \text{ mV/MPa}$, the electric field within the thrust will be 0.04 mV/m . This electric field could be measured in different boreholes when they intercept the same thrust. For example, if the distance between P'_1 and P_1 is 300 m , we could expect to measure $V_1 - V'_1 = 12 \text{ mV}$. The electric field can be monitored in the same well intercepting several thrusts. Thus we would be able to detect any difference of pressure gradients in the different thrusts considered.

The pressure gradient is a key factor needed to compute the electric field, since the electric field is directly proportional to the pressure field. We could even imagine that if there exists an overpressure in a homogeneous formation (no thrust), then an electric field will be induced. If we consider now that the pressure gradient along the thrust is closer to lithostatic [Moore, 1989] $\Delta P/\Delta Y = 30 \text{ MPa/km}$, J_{conv} is therefore 3 times greater than the calculation considered in the first case and $B_x = 0.21 \text{ nT}$.

Above and below the thrusts we could thus detect 0.42 nT . In the second case the electric field within the thrusts will be 0.12 mV/m . The electric current density is a key factor for computing the magnetic field since the magnetic field is directly proportional to this current density.

Since the real configuration will be included between the two extreme cases and the two pressure gradients (hydrostatic and lithostatic), we show here that the fluid circulation within thrusts could induce a maximum horizontal magnetic field of the order of 0.4 nT and a maximum electric field along the thrust of the order of 0.12 mV/m . We now develop a more realistic model which takes into account the coupled system of convection and conduction currents.

3.2. Numerical Model

This model proceeds in three steps: first, the hydraulic flow circulation is computed using Darcy's law; second, the streaming potential and current density are computed using Helmholtz-Smoluchowski's law and the pressure gradient from the previous hydraulic step; and third, the magnetic field is obtained from the Biot-Savart law and the electric current densities are obtained from the previous electrokinetic step. Our approach is very different from that of Heinson and Segawa [1997] since modeling the porosity reduction within the prism, they showed that décollement permeability has to be very high, and they computed the seafloor electric potential.

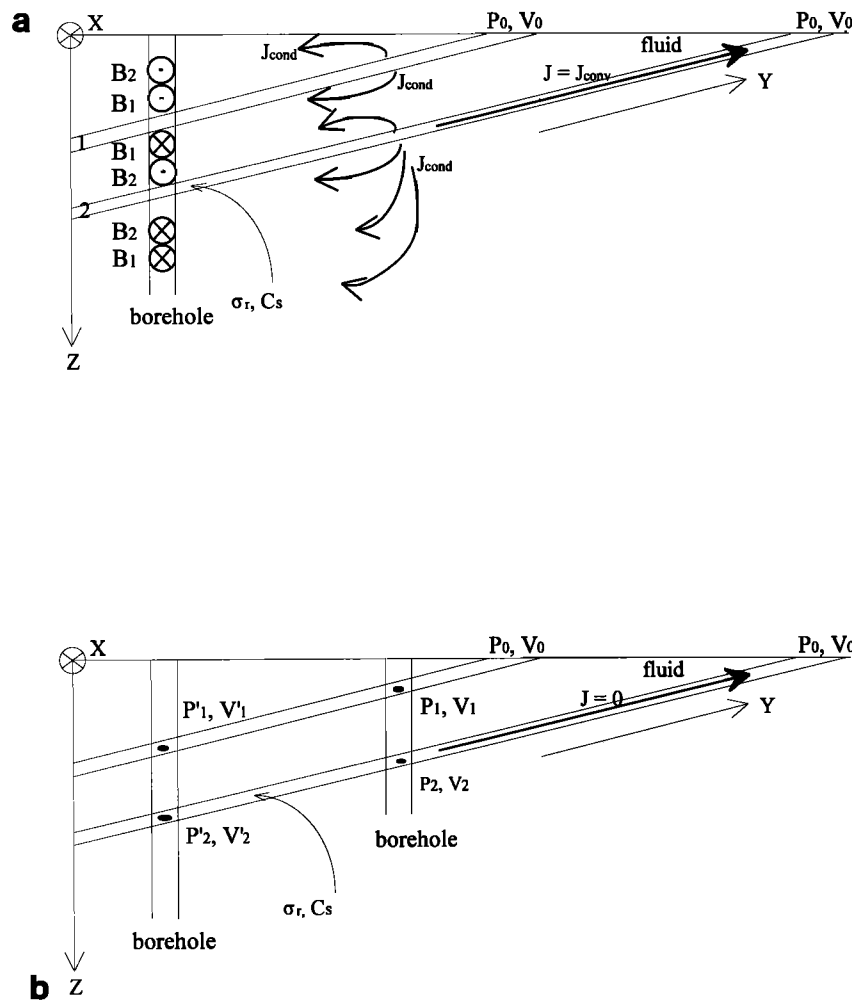


Figure 2. Geometry of the thrusts and borehole considered for the analytic model. P is the pressure and V is the electric potential. B is the magnetic field induced by fluid flow and is perpendicular to the figure. J_{cond} is the conduction current density. The total current density within the thrust is assumed (a) to be the convection density J_{conv} or (b) to be zero.

3.2.1. Geometry of the model. Hydraulic flow and electric current are modeled in a system of thrust faults connecting the décollement zone to the seafloor. The geometry of faults has been chosen from a seismic reflection study in the Nankai region seafloor from Moore *et al.* [1990] (Figure 3a). The subhorizontal interpreted reflector is a sedimentary horizon that has been disrupted by the thrust faulting. The thrust faults are spaced at 2 km. In the model the thickness of the ocean sediment is 1000 m above the décollement which is at the bottom, and the ocean above has a depth of 1000 m. The décollement is modeled as 50 m wide, and the faults are modeled as 10 m wide; the total lateral dimension investigated by the model is 48 km. The model is two-dimensional Cartesian and is shown in Figure 3b.

3.2.2. Physical parameters. Our model of fluid flow within an accretionary prism uses Darcy's law with matrix and faults being assigned different permeabilities. We consider different parts in the Nankai accretionary prism with different physical properties: the décollement and faults which are permeable and where most of the fluid flow takes place; the sediments which are less permeable and more conductive. The sediments above the near-horizontal reflector, called reflector A, are bedded sand, silt turbidites, and hemipelagic mud, whereas the sediments below

the near-horizontal reflector are ash/tuff and hemipelagic mud [Winkler and Stewart, 1991]. Permeability data from accretionary prisms are limited to measurements from small samples and large scale inferences from their matrix or intergranular permeability range from 10^{-20} m² to 10^{-13} m² [Moore and Vrolijk, 1992]. Permeability of sediments above the reflector is about 2×10^{-15} m², and permeability of sediments below the reflector is about 5×10^{-17} m² [Taylor and Fisher, 1993]. The décollement zone is maintained by high fluid pressure [Westbrook *et al.*, 1982] and acts as a major conduit for fluid expulsion [Cloos, 1984; Moore *et al.*, 1987], and high fracture permeability is assumed to allow flow along the décollement [Moore, 1989]. Focused fluid flow is 3 to 5 orders of magnitude larger than distributed flow, probably representing the mean difference in permeability along these respective expulsion paths [Screaton *et al.*, 1990; Henry and Le Pichon, 1991; Moore and Vrolijk, 1992]. At the Barbados accretionary complex, observations of heat flow suggested high permeability (10^{-12} m²) within the décollement zone [Fisher and Hounslow, 1990]. Moreover, Heinson and Segawa [1997] showed that permeability of the décollement must be ~4 orders of magnitude bigger than the permeability within the adjacent sediments to

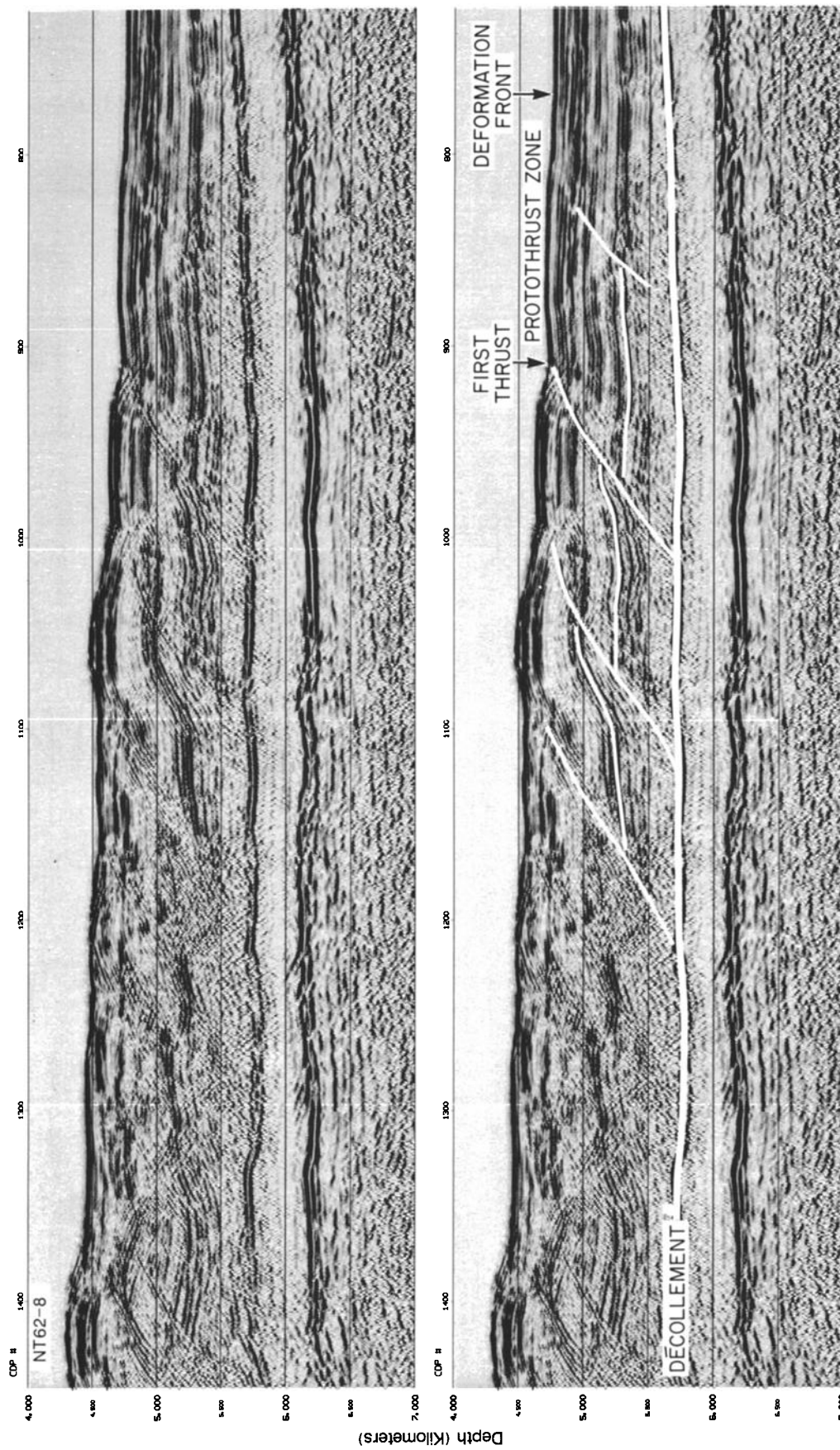


Figure 3a. Seismic profile on Nankai prism from Moore *et al.* [1990].

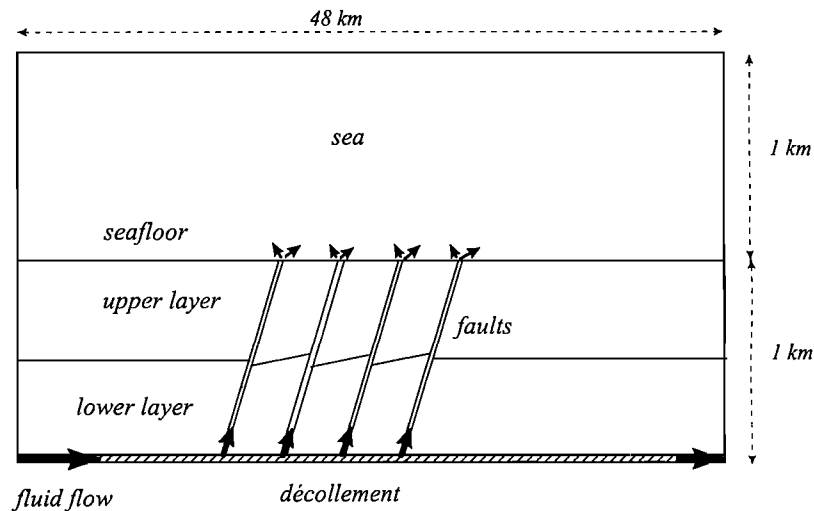


Figure 3b. Scheme of the model geometry. Lateral positions of the faults in the décollement are 20.1, 22.1, 24.1, and 26.1 km from the fluid source, and lateral positions of the vents at the seafloor are 22, 24, 26, and 28 km from the fluid source.

produce observed fluid flow. Permeability has been chosen equal to 10^{-13} m^2 in faults and $3.5 \times 10^{-13} \text{ m}^2$ in the décollement. Therefore the difference in permeabilities between the décollement and the sediments is ~ 2 orders of magnitude for the sediments above reflector A and ~ 4 orders of magnitude for the sediments below reflector A. Permeabilities are assumed to be isotropic.

Geometry of the electric current path is governed by the contrast between the electric conductivity in the décollement and in the thrusts and the electric conductivity in the rest of the sediments. Formation factor F , which is the rock resistivity divided by the fluid resistivity, is therefore different in the faults and in the décollement and in the adjacent sediments. Sediments above reflector A have an average porosity Φ of 45%, while sediments below reflector A have an average porosity of 35% [Hyndman *et al.*, 1993; Moran *et al.*, 1993]. Porosity in the décollement zone is $\sim 25\%$ [Hyndman *et al.*, 1993], and porosity in the thrust faults has also been chosen equal to 25%. Formation factor F has been deduced from the equation $F = (3.8/\Phi)^{1.14}$ –4.755 [Taira *et al.*, 1990] and is equal to 6.6 in sediments above reflector A and is equal to 10 below this reflector. In the thrust faults and in the décollement, formation factor is equal to 17.

The electric conductivity of the fluid σ_f is that of seawater inside the sediments above reflector A: $\sigma_f = 5.3 \text{ S/m}$. As the chlorinity concentration has been shown to decrease with depth up to 20% at the décollement depth [Gieskes *et al.*, 1993; Kastner *et al.*, 1993], an average decrease of 10% in the fluid conductivity has been taken into account below the reflector A: $\sigma_f = 4.8 \text{ S/m}$. A decrease of 20% has been taken into account

within the décollement: $\sigma_f = 4.2 \text{ S/m}$. Within the décollement the electrical conductivity is $\sigma_r = \sigma_f/F = 0.25 \text{ S/m}$, below reflector A, $\sigma_r = 0.48 \text{ S/m}$, above reflector A, $\sigma_r = 0.80 \text{ S/m}$, and within the thrusts, $\sigma_r = 0.31 \text{ S/m}$. Note that since the porosity is lower within the thrusts and décollement than within the adjacent sediments, the conductivity is lower within the thrusts and décollement than within the adjacent sediments, although the permeability is larger [Langseth and Moore, 1990]. The physical parameters are summarized in Table 1. Our approach is different than the one from Heinson and Segawa [1997] since they considered only a change in permeability through the décollement compared to the prism sediment and assumed conductivity as a function of depth without special change through the décollement.

The zeta potential (equation (2)) reflects the interaction between the fluid and the matrix, and it depends on many parameters such as the nature of fluids (ions concentration, conductivity, pH, temperature) and the nature of rocks (mineralogy, surface conductivity). In subduction zones, most sediments are terrigenous clastic deposits containing clay minerals such as smectite or illite. Streaming potential is usually investigated in quartz-water systems [Ishido and Mizutani, 1981], on sands and sandstones [Sharma *et al.*, 1987; Jouniaux and Pozzi, 1995a, 1997; Lorne *et al.*, 1998a, 1998b] or on limestones [Jouniaux and Pozzi, 1995b; Jouniaux *et al.*, 1996]. For a quartz system with NaCl solution the zeta potential is expected to be equal to -25 mV for a concentration of 10^{-1} mol/L corresponding to a conductivity of 1 S/m [Pride and Morgan, 1991; Revil and Glover, 1997]. Measurements of zeta potential by electrophoresis on kaolinite showed a zeta potential of about -32 mV with a solution of NaCl 10^{-1} mol/L for a pH 5.5 to 7.5 [Poirier and Cases, 1985].

The effect of temperature on the zeta potential is still controversial as only few studies are available [Somasundaran and Kulkarni, 1973; Ishido and Mizutani, 1981]; as a consequence, the zeta potential has been considered to be constant in our model without taking into account the effect of a thermal gradient. Moreover, the effect of methane detected in variable concentrations in fluids [Moore and Vrolijk, 1992] is not known on the zeta potential. In our model the zeta potential has

Table 1. Physical Parameters for the Model

| | $k, \text{ m}^2$ | Porosity, % | F | $\sigma_r, \text{ S/m}$ |
|-------------|-----------------------|-------------|---------|-------------------------|
| Sea | | | | 5.3 |
| Upper layer | 10^{-15} | 45 | 6.6 | 5.3 |
| Lower layer | 5×10^{-17} | 35 | 10 | 4.8 |
| Décollement | 3.5×10^{-13} | 25 | 17 or 6 | 4.2 |
| Fault | 10^{-13} | 25 | 17 or 6 | 5.3 |

therefore been chosen as constant and equal to -30 mV. This value leads to an electrokinetic coupling coefficient (equation (2)) $C_s = -4$ mV/MPa (with $\epsilon = 7 \times 10^{-10}$ F/m, $\eta = 10^{-3}$ Pa s, and $\sigma_f = 4.8$ S/m).

3.2.3. Three-step modeling. Electromagnetic models of electrokinetic phenomena require coupled modeling of fluid flow, electric (streaming) potential and magnetic field. The coupling of the potential gradient with the pressure gradient is taken into account. The electroosmotic coefficient term is negligible [Fitterman, 1978], leading to Darcy's law for the fluid flow. Such an approach has been implemented in the FLUX-EXPERT generation system "open codes" where an equation or a system of differential equations can be introduced by the user [Massé and Berthier, 1995, 1996] using the following options: second-order curvilinear finite elements, second-order curvilinear boundary elements, Gauss-Legendre approximations for integral calculations, Lagrangian second-order polynomials for test and interpolation functions, and incomplete Cholesky conjugate gradient method for solving linear systems.

3.2.3.1. Hydraulic modeling: The fluid is presumed to be injected into the décollement at the left of the model, and it flows within the décollement, the thrusts, and the sediments. The flow rate of water entering the décollement fault at its left end and exiting at its right end is not exactly known and is used here as a source to create fluid flow inside the thrusts. It is assumed that fluid velocities entering and exiting the décollement are 50 and 25 m/yr respectively, because these values will be shown to produce reasonable Darcian fluid flow velocities at the fault outlets on the seafloor. The model considered here is a steady state model.

Inside porous media the flow of water is sufficiently slow so that it is ruled by Darcy's law where the permeability coefficient is a tensor

$$u = -\frac{[k]}{\eta} \text{grad } P \quad (5)$$

where u is the Darcy fluid velocity, P is the pressure, and $[k]$ is the permeability tensor. The pressure gradient inducing the flow is either steady or slowly oscillating at a low frequency so that inertial effects are small compared to viscous ones. Taking into account the conservation of the flow rate, (5) yields

$$\text{div}\left(-\frac{[k]}{\eta} \text{grad } P\right) = 0 \quad (6)$$

The pressure computed here is in reality the excess pore pressure, meaning the pressure difference between total pressure and hydrostatic pressure.

To solve for the pressure, boundary conditions are needed either on the pressure itself or on the flux $F = -(k/\eta) \text{grad } P \cdot n$, where n is the vector normal to the fluid inlet. An initial state must be given for the pressure at the initial time step. At the boundaries of media of different properties, the mass flow is conserved, i.e.,

$$\rho_1 \frac{[k_1]}{\eta} \text{grad } P_{n1} = \rho_2 \frac{[k_2]}{\eta} \text{grad } P_{n2} \quad (7)$$

Boundary conditions for the excess pressure are zero at the two lateral ends inside the sea domain. There is no fluid flow perpendicular to the lateral sides in the sediments ($dP/dn = 0$) and no flow perpendicular to the bottom of the décollement ($dP/dn' = 0$, n' being the normal to the bottom). The sea is

modeled as a medium of high permeability ($k = 5 \times 10^{-9}$ m²) which was determined only by consideration of convergence of the numerical system and not on a physical ground, since the fluid velocities inside the sea do not produce any electrokinetic phenomena. The dynamic viscosity of water is presumed constant in the whole computational domain and equal to 10^{-3} Pa s. Once the fluid pressure field has been calculated the Darcian fluid velocities are obtained from (5).

3.2.3.2. Streaming potential modeling: The frequency of the pressure oscillations being very low, the electromagnetic field conforms to the Maxwell equations in their static approximations (<100 Hz). The electric field being irrotational, it is given by $E = -\text{grad } V$, where V is the electric scalar potential. Ohm's law states that the current density J is the sum of a conduction current and a convection current $J = \sigma_f E + \rho_e u$, where ρ_e is the electric charge. Then using (7) and the Debye approximation for the double layer [Overbeek, 1952], one obtains the Helmholtz-Smoluchowski expression for the total current density J :

$$J = -[G] \sigma_f \text{grad } V + [G] \frac{\epsilon \zeta}{\eta} \text{grad } P \quad (8)$$

where $[G]$ is a geometrical tensor linked to the global conductivity σ_r and fluid conductivity σ_f by the relation $\sigma_r = [G] \sigma_f$ (G is the inverse of the formation factor F). In our application the pressure gradient is the source term, and the streaming potential V is the response to this source. Using the current conservation equation $\text{div } J = 0$, (8) can be written in the form

$$\text{div}([G] \sigma_f \text{grad } V) = \text{div}([G] \frac{\epsilon \zeta}{\eta} \text{grad } P) \quad (9)$$

The coefficients G , ζ , σ_f , η , and ϵ have been kept inside the divergence because they are allowed to change spatially. At a boundary between two porous media the following relation holds:

$$\begin{aligned} -[G_1] \sigma_f \text{grad } V_{n1} + [G_1] \frac{\epsilon \zeta}{\eta} \text{grad } P_{n1} - [G_2] \sigma_f \text{grad } V_{n2} \\ + [G_2] \frac{\epsilon \zeta}{\eta} \text{grad } P_{n2} = 0 \end{aligned}$$

The electrokinetic step has been divided into two consecutive substeps:

First, the streaming potential V is solved in (9) by considering only the part of the domain below the seafloor. The boundary conditions for V are then $V=0$ at the seafloor (this hypothesis will be shown to be valid at the next substep). On the lateral sides of the sediments the electric current is vertical ($dV/dn = 0$), and at the bottom of the décollement the current is horizontal ($dV/dn' = 0$). The potential is assumed uniform within the thickness of the décollement where the flow enters and exits the domain.

Second, the electric potential is computed in the sea using the electric current densities computed on the seafloor in the previous step and solving the equation $\text{div}(\sigma_f \text{grad } V) = 0$. The potential is considered equal to zero at the two lateral ends of the sea region. Such an approach ensures the conservation of the electric current density J at the seafloor, but a very slight discontinuity is observed in the potential V . However, the discontinuity is negligible since the potential in the sea is about 1000 times less than the potential under the seafloor. If the

potential computed at the seafloor is now taken as the limit boundary in order to compute the potential in the sediments, the results are not different.

3.2.3.3. Magnetic field modeling: The Maxwell laws in a quasi-static expression are $\text{curl } H = J$ and $\text{div } B = 0$, where H is the magnetic field (A/m) and B is the magnetic induction (in tesla). We can define a potential vector A such as $B = \text{curl } A$ and choose the Coulomb gauge $\text{div } A = 0$. Recalling that $B = \mu H$, where μ is the magnetic permeability, the potential vector satisfies the relations $\text{div } A = 0$, and the Biot-Savart law

$$\text{curl}\left(\frac{1}{\mu} \text{curl } A\right) = -[G]\sigma_f \text{grad } V + [G]\frac{\varepsilon\zeta}{\eta} \text{grad } P \quad (10)$$

The current densities J have been computed in the previous step for the whole computational domain. The natural boundary conditions between two different media are $(1/\mu_1)\text{curl } A \wedge n_1 + (1/\mu_2)\text{curl } A \wedge n_2 = 0$ and $A = 0$ at infinity.

The vector potential A is obtained by solving (10) with the following boundary conditions: $A_x = A_y = 0$ at the sea surface and at the two lateral ends of the computational domain. $A_x = 0$ at the lower boundary (below the décollement). The first boundary condition is valid only if the electric currents circulating outside the computational domain do not contribute to the magnetic field inside the domain. It is clear that such a hypothesis is not valid inside the domain close to the boundaries, but as we chose a large computational domain and as the level of the magnetic field is small (as will be shown in section 4.3), this hypothesis seems reasonable for the calculation in a restricted domain around the faulted zone. The second boundary condition is simply the consequence of no electric currents circulating downward from the décollement. The value of the magnetic permeability is constant over the whole domain and equal to that of a vacuum. As the calculation is two-dimensional, there exists only one component (normal to the domain) of the magnetic field.

4. Results

The results have been plotted in Plates 1-6 and Figures 4-6.

4.1. Fluid Circulation

The excess fluid pressure in the accretionary prism has been plotted over the whole computational domain in Plate 1a and in the fault system in Plate 1b. The pressure source is localized on the left side of the décollement. The numerical results show an excess pressure gradient inside the thrust faults of ~ 10 MPa/km. Fluid pressures in accretionary prisms are commonly high but range from hydrostatic to lithostatic [Moore, 1989]. At shallow depth the pressure gradient is thought to be almost hydrostatic (10 MPa/km) [Moore, 1989], meaning an excess pressure gradient near zero. Temperature measurements below clam colonies on the Nankai accretionary prism showed an excess pore pressure gradient of 10 Pa/m over 1-2 m depth [Henry et al., 1992]. At depth the pressure gradient is closer to the lithostatic gradient (about 30 MPa/km) [Moore, 1989], meaning an excess pore pressure gradient of ~ 20 MPa/km. The Hubbert and Rubey [1959] dimensionless parameter λ , defined as the fluid pressure P_f divided by the vertical stress σ_z exerted by the lithostatic overburden $\lambda = P_f / \sigma_z$, allows us to quantify the overpressure. The graph of pressure from Moore [1989, Figure 10] shows λ of ~ 0.75 near the décollement and ~ 0.6 at a depth half that of the décollement (let us say 500 m depth in our case). Westbrook et

al. [1982] reported that the low stresses required on the décollement on the lesser Antilles subduction zone are made possible by pore water within the décollement at pressure close to that of the lithostatic load ($\lambda = 0.81$ to 0.97). Water pressures approximately equivalent to the lithostatic load were inferred close to the décollement on the Barbados ridge complex [Westbrook and Smith, 1983]. Fluid pressures at near lithostatic values are also invoked to develop laterally extensive fractureways filled with dewatering fluids derived from deeper underthrust water-rich sediments [Cloos, 1984]. The pore fluid pressure ratio of Hubbert and Rubey [1959] has been generalized to the case of a submarine wedge [Davis et al., 1983]: $\lambda = (P_f - \rho_w g D) / (\sigma_z - \rho_w g D)$, where $\rho_w g D$ is the hydrostatic pressure at the seafloor (10 MPa in our case since the seafloor is at 1 km depth). This parameter is equal to 1 when fluid pressure is equal to the lithostatic pressure and equal to ~ 0.4 when the fluid pressure is equal to the hydrostatic pressure. This coefficient has been predicted for various accretionary wedges from the pressure-dependent Coulomb wedge theory and has been shown to be ~ 0.7 - 0.9 [Davis et al., 1983]. Recent study of the décollement propagation as a subhorizontal tension fracture requires also high pore pressure within the décollement [Morgan and Karig, 1995]. It seems therefore that λ of ~ 0.7 - 0.9 is considered as a reasonable value within the décollement. The value of λ deduced from our model is plotted in Figure 4. The λ values range from 0.65 to 1 within the décollement in the faults domain. Note that it is not the scope of this paper to deal with hydrofracture and that the realistic model is represented by the faults domain, not near the boundaries of the whole computational domain.

The distribution of the fluid velocity in the second fault is shown in Plate 2 in which the velocity vector has been plotted. The fluid velocity is of the order of 1 m/yr at the output of the thrust. Note that the upward Darcian fluid flow velocity in the Nankai region has been deduced from temperature measurements and has been found to be of the order of 10 m/yr at some fluid venting at the seafloor and of the order of 100 m/yr above the most active faults [Le Pichon et al., 1992; Henry et al., 1992]. The threshold of detection of the Darcian velocities deduced from these temperature measurements is 10 m/yr [Henry et al., 1992], so that our computed values of the order of 1 m/yr seem to be reasonable values.

4.2. Streaming Potential

The electric potential repartition has been plotted in Plate 3a for the whole computational domain and for an enlargement of the fault zone in Plate 3b. The electric potential at the seafloor is constant and is < 1 mV in absolute value. As a consequence, the horizontal electric field is zero at the seafloor.

The electric potential increases with depth (in absolute value) up to > 45 mV near the décollement at the second fault. The electric potential has been plotted versus depth in Figure 5, just above the the second vent (squares) (lateral position 24,000 m in Plate 3b), and between the first and second vent (triangles) (lateral position 23,000 m in Plate 3b). The potential increases with depth, and the result of the least squares regression for the first 500 m depth shows that the potential is given by $V(\text{mV}) = -0.9 - 0.005x D_{\text{epth}}(\text{m})$ and $V(\text{mV}) = 1.3 - 0.026x D_{\text{epth}}(\text{m})$ for profiles above the vent and between the vents, respectively. Therefore the rate of potential increase with depth is larger when along a profile between two vents. Below reflector A at ~ 500 m depth, the rate of potential increase is larger, because the medium is less conductive (Figure 3 and Table 1), and the vertical electric field is between 90 and 100 mV/km (Figure 5). Note that far from the

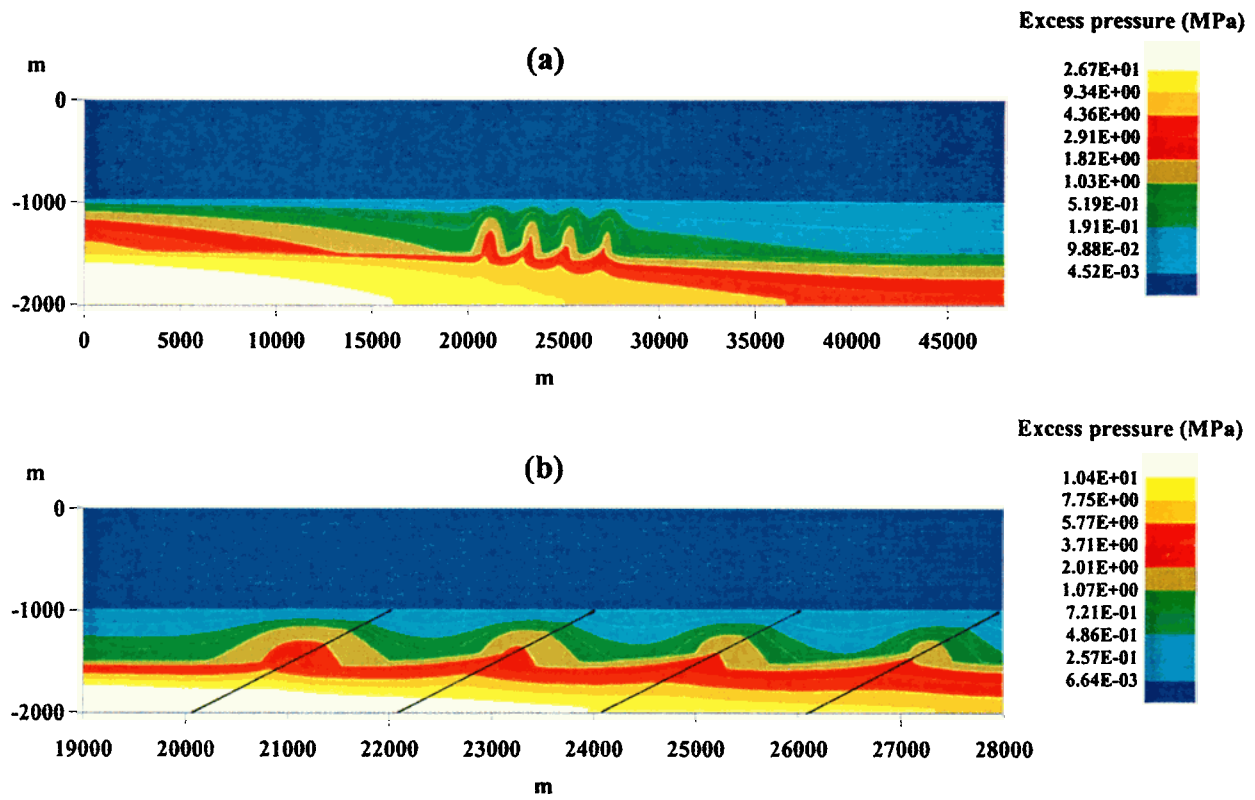


Plate 1. Pressure distribution (a) in the whole computational domain (48 km large) and (b) in the four thrusts domain (9 km large). The seafloor level is at -1000 m.

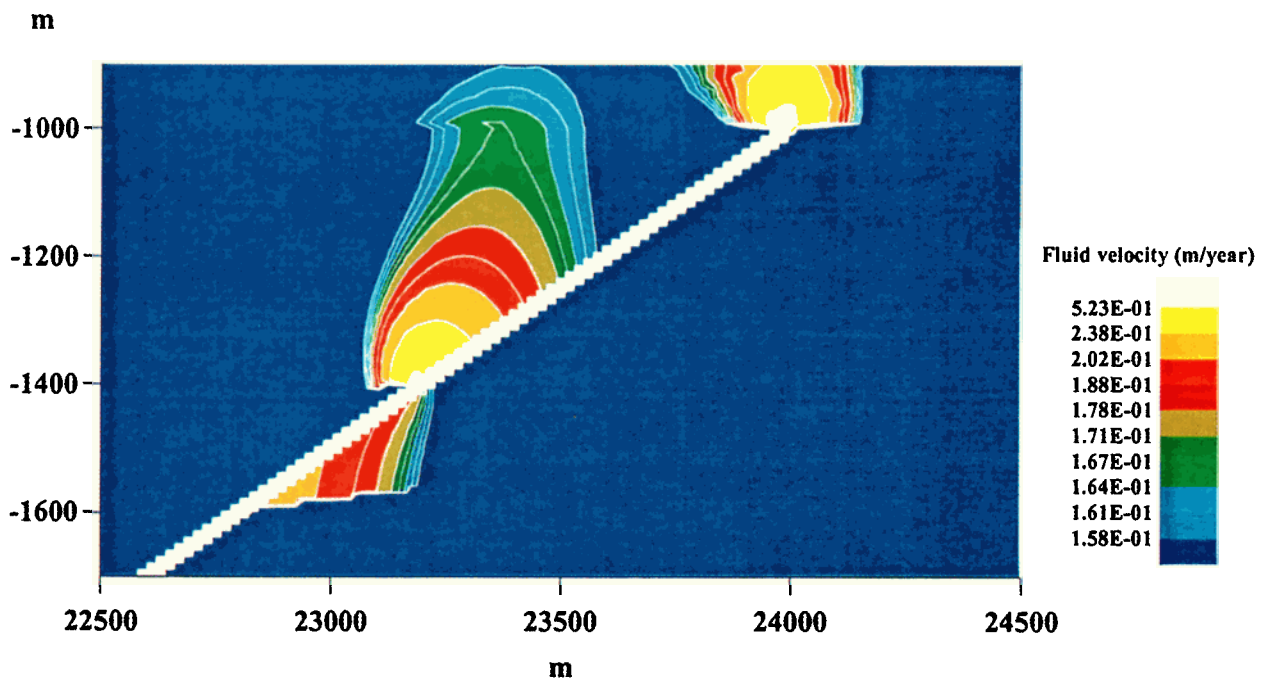


Plate 2. Distribution of fluid velocity within the second thrust (lateral location from 22.5 km to 24.5 km). The seafloor level is at -1000 m.

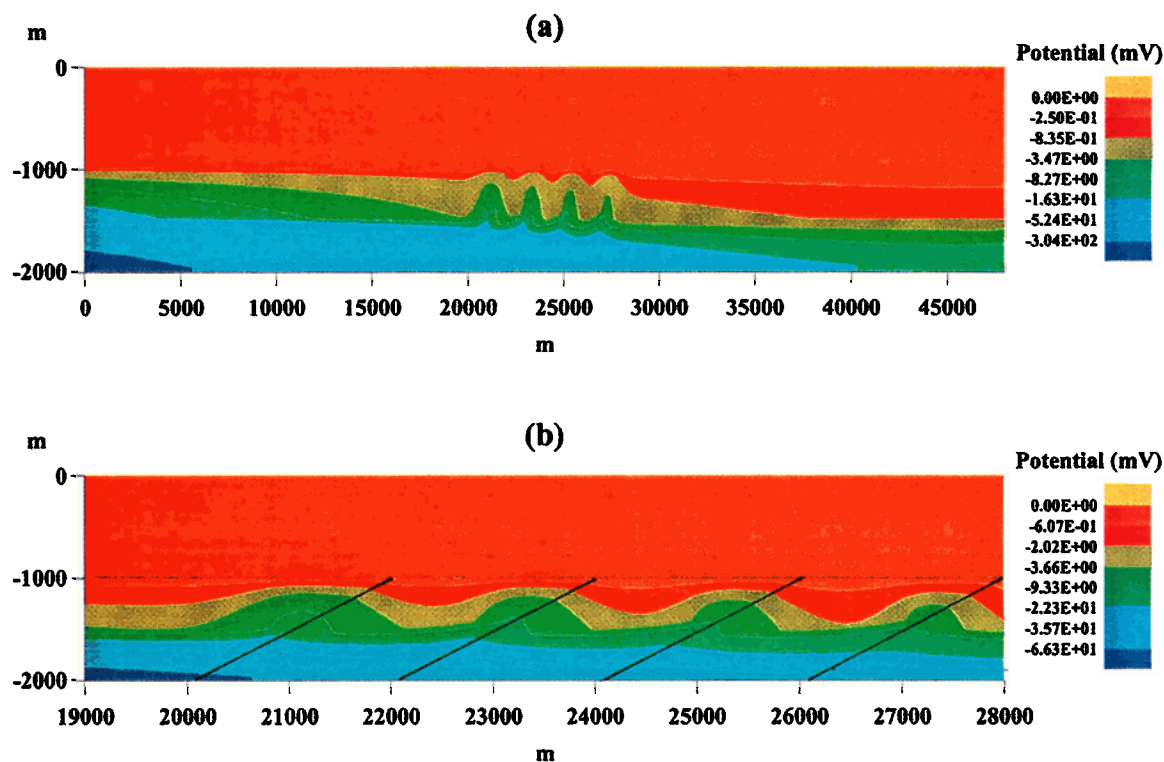


Plate 3. Streaming potential distribution (a) in the whole computational domain (48 km large) and (b) in the four thrusts domain (9 km large). The seafloor level is at -1000 m.

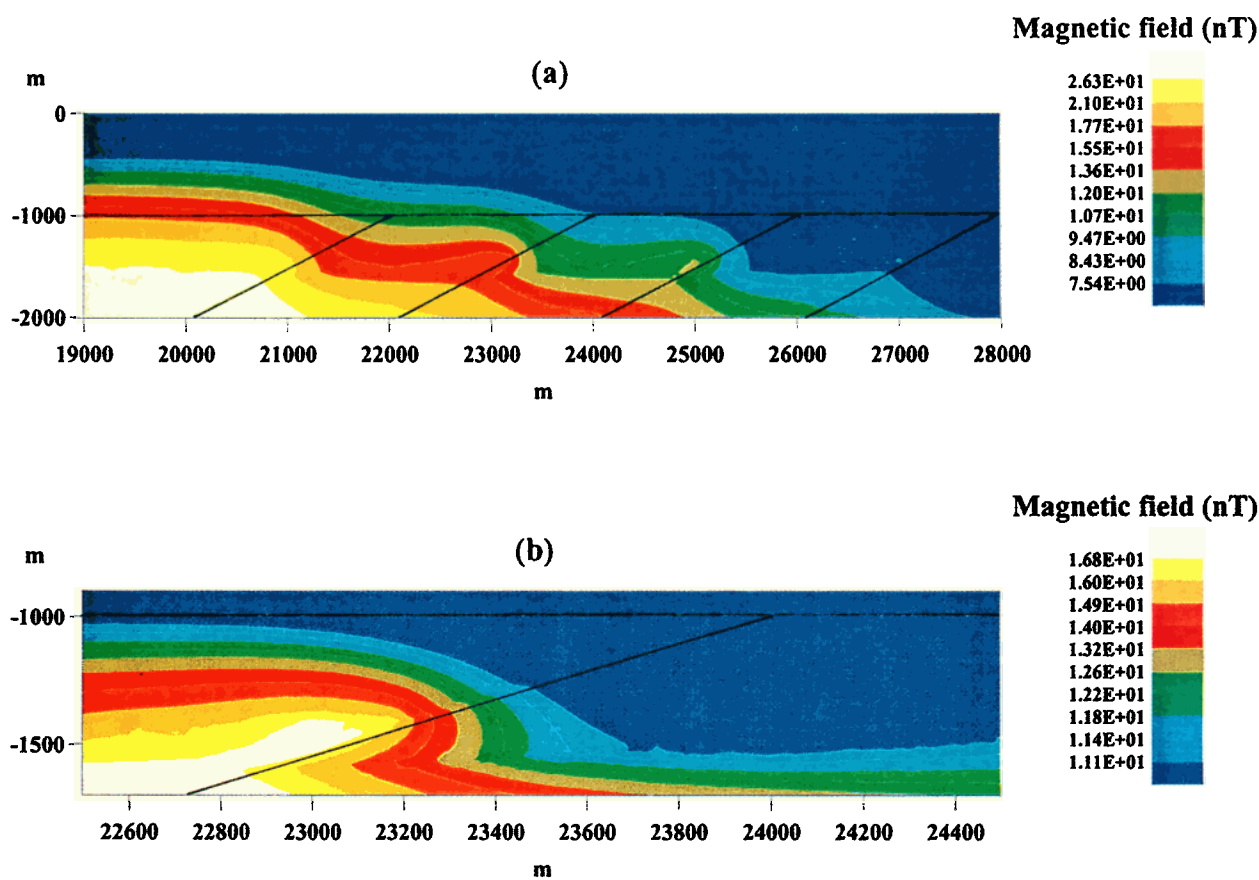


Plate 4. Distribution of the magnetic field (a) in the four thrusts domain and (b) in an enlargement in the vicinity of the second thrust. Seafloor level is at -1000 m.

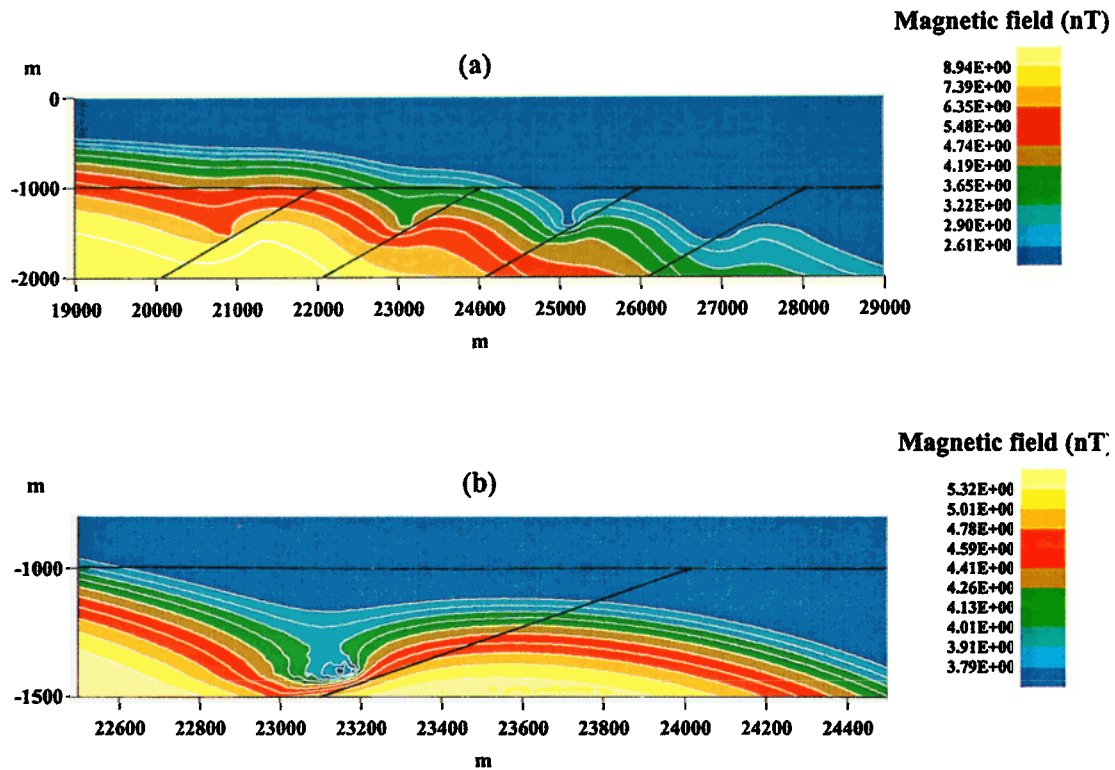


Plate 5. Distribution of the magnetic field in the case where the rock conductivity within the faults and in the décollement (décollement width is 50 m) is larger than in the surrounding sediments, (a) in the four thrusts domain and (b) in an enlargement in the vicinity of the second thrust. Seafloor level is at -1000 m.

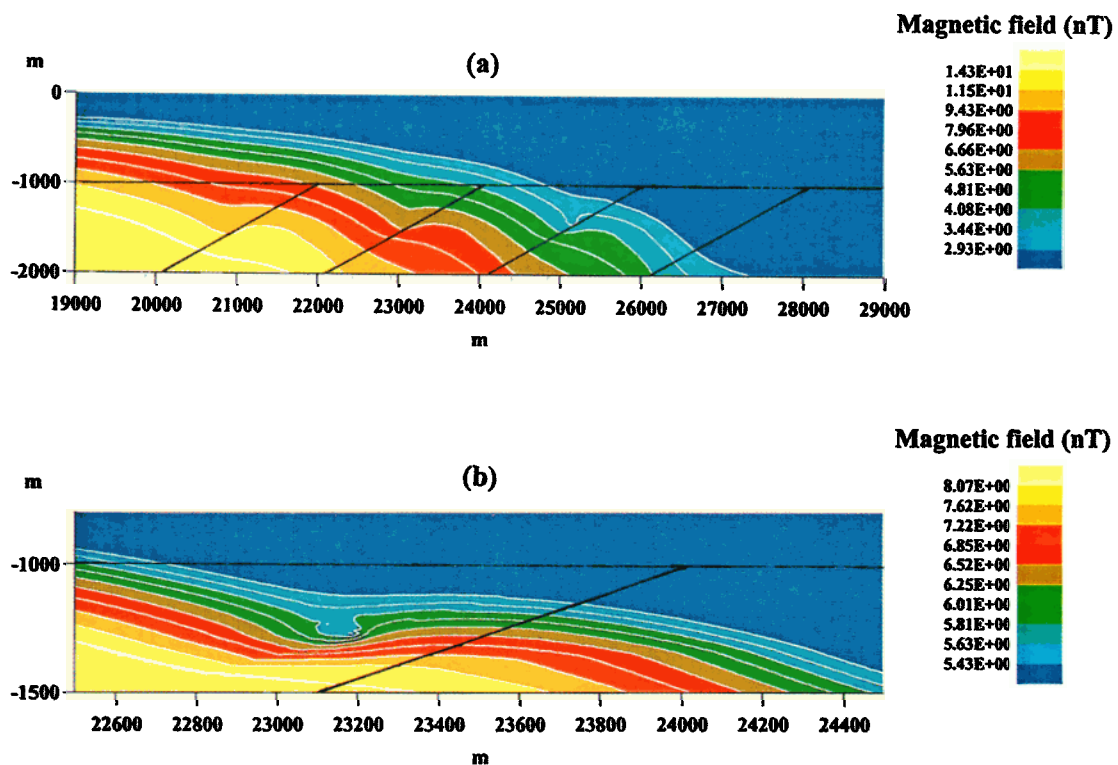


Plate 6. Distribution of the magnetic field when the décollement width is 20 m and in the case where the rock conductivity within the faults and in the décollement is larger than in the surrounding sediments, (a) in the four thrusts domain and (b) in an enlargement in the vicinity of the second thrust. Seafloor level is at -1000 m.

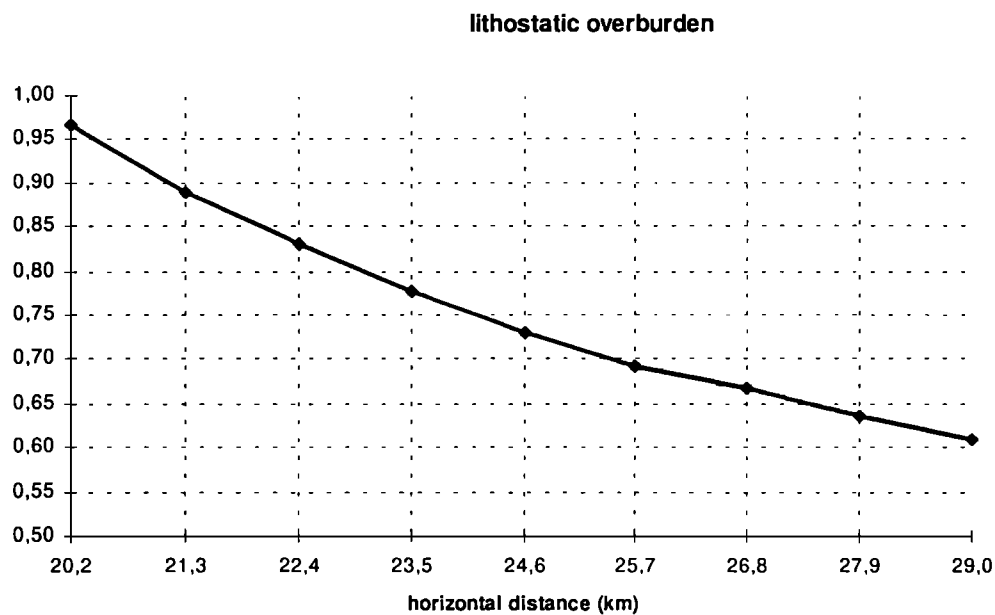


Figure 4. Values of the coefficient λ within the décollement in the thrusts domain for lateral position from 20.2 to 29 km.

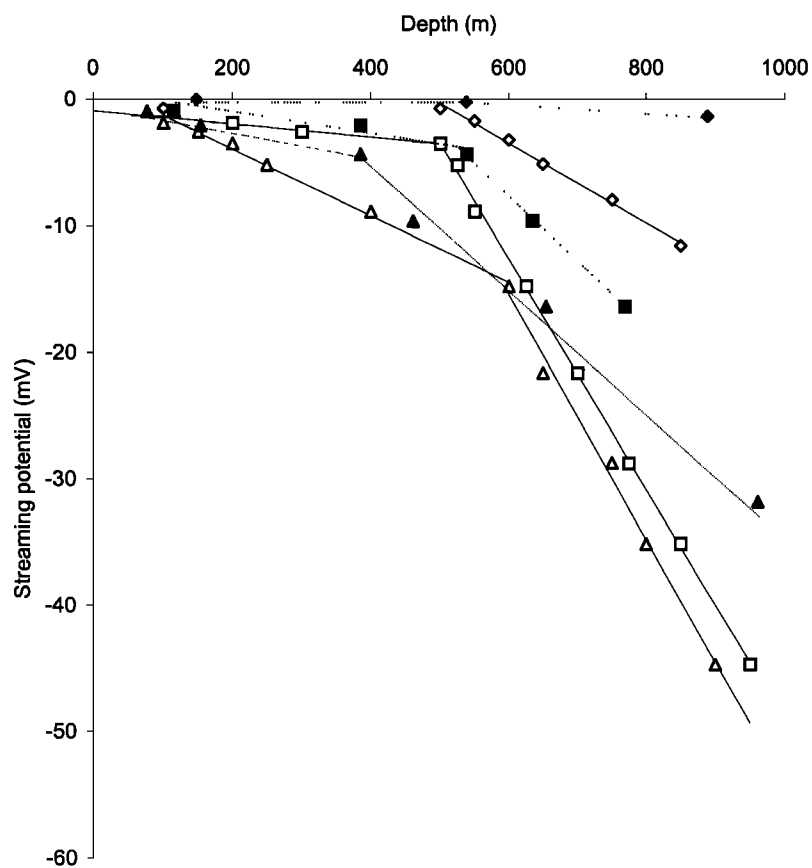


Figure 5. Streaming potential versus depth (below the seafloor) for lateral positions 24,000 m (squares) and 23,000 m (triangles), which are above the second vent and between the first and second vent, and for lateral position 45 km (diamonds) which is far from the source. Open symbols are for the case when $F=17$ in the décollement and in the faults and when the décollement width is 50 m. Solid symbols are for the case when $F=6$ in the décollement and in the faults and when the décollement width is 20 m.

fluid source, at 45 km, for example (Plate 3a) the vertical electric field is zero up to reflector A (Figure 5, diamonds) and of ~ 31 mV/km below this reflector A.

Because we take into account the conduction current in our model, we find a small current density of the order of $0.5\text{--}2 \times 10^{-5}$ A/m², since the back current is opposite to the convection current. The faults clearly drain the electric current through the domain from the décollement to the sea.

4.3. Magnetic Field

The current density computed by our model is localized in the vertical plane, as the calculation is two-dimensional, and the magnetic field due to this current density will have a component perpendicular to this vertical plane. The horizontal magnetic field anomaly is shown in Plate 4a for the fault domain and in Plate 4b for the second fault.

The horizontal variation of the magnetic field at the seafloor is shown in Figure 6. The horizontal gradient of the magnetic field is ~ 2 nT/km at the seafloor in the faults domain (Figure 6). The vertical variation of the magnetic field above the second vent (lateral distance 24,000 m in Plate 4a) and between the first and second vent (lateral distance 23,000 m in Plate 4a) is shown Figure 6 (squares and triangles, respectively). The magnetic field increases with depth and for the first 400 m depth the magnetic field is given by $B(\text{nT}) = 7.6 + 0.0077 \times D_{\text{epth}}(\text{m})$ and $B(\text{nT}) =$

$9.3 + 0.0149 \times D_{\text{epth}}(\text{m})$ (open symbols) for profiles above the vent (squares) and between the vents (triangles), respectively. Therefore the rate of magnetic field increase with depth is larger between two vents. Then the rate of increase of the magnetic field is decreased around the 500 m depth where reflector A is located. The magnetic field is even constant between 400 and 700 m depth for the profile made between two vents since the isovalues of the field are distorted (Plate 4). Then the vertical gradient of the magnetic field is 11 nT/km at depth (Figure 6, open symbols). Note that far from the fluid source the vertical gradient of the magnetic field is zero (Plate 4a).

The model has been calculated with the physical parameters discussed above. In this paragraph we analyze the stability of the streaming potential against the possible variation of these parameters. As shown by Plates 1 and 3 the streaming potential reflects directly the excess pressure within the prism. If the pressure gradient is multiplied, for instance, by 2, the same increase is expected in the streaming potential (see equation (9)). If the fluid conductivity is decreased by 20% as discussed above, then the streaming potential is expected to be increased by 20% (see equation (9)). The streaming potential is proportional to the zeta potential within the electric double layer. The zeta potential is deduced from available measurements on a quartz-water system and kaolinite. Better constrained values can be expected from further experimental work [than Jouniaux *et al.*, 1994] on proper rocks from an accretionary prism.

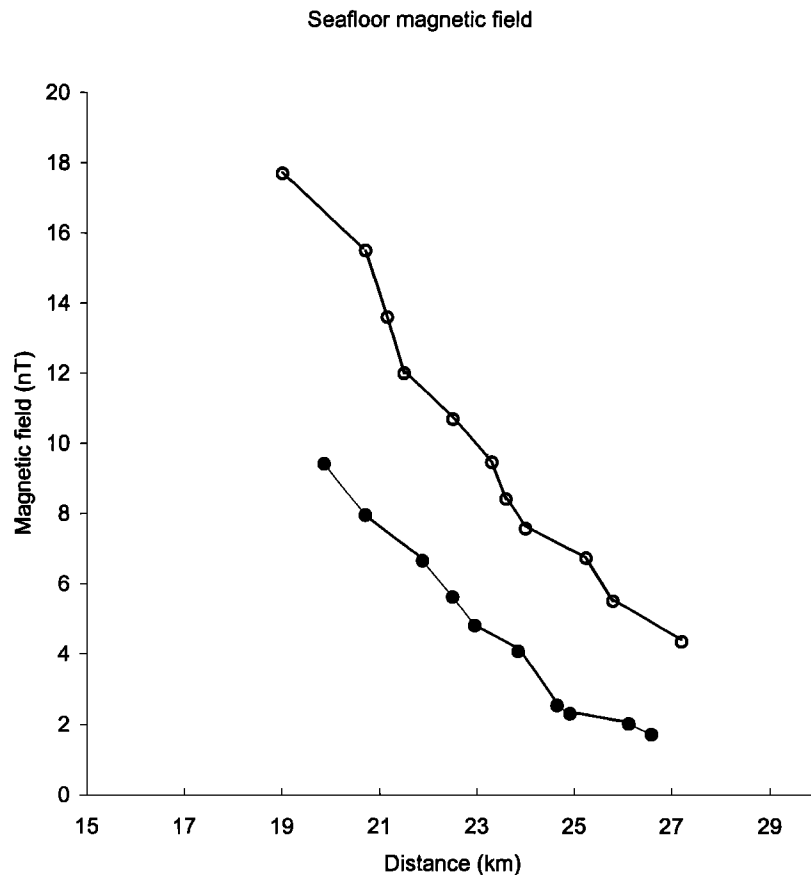


Figure 6a. Magnetic field at the seafloor for lateral positions from 19 to 27 km. Open symbols are for the case when $F=17$ in the décollement and in the faults and when the décollement width is 50 m. Solid symbols are for the case when $F=6$ in the décollement and in the faults and when the décollement width is 20 m.

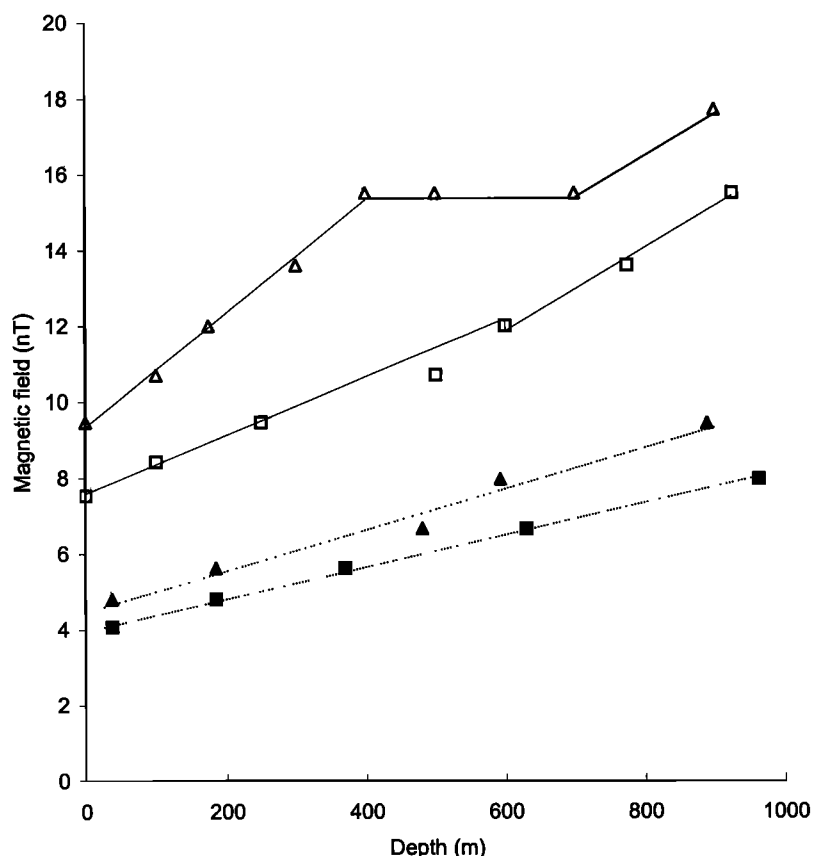


Figure 6b. Magnetic field versus depth (below the seafloor) for lateral positions 24,000 m (squares) and 23,000 m (triangles), which are above the second vent and between the first and second vent. Open symbols are for the case when $F=17$ in the décollement and in the faults and when the décollement width is 50 m. Solid symbols are for the case when $F=6$ in the décollement and in the faults and when the décollement width is 20 m.

4.4. Effect of Décollement Width and Conductivity

Since the permeability is higher in the faults and in the décollement because of fracture porosity, it might be possible that the conductivity is anomalously high along the fault and décollement and that the relationship between porosity and conductivity (described in section 3.2.2) is not appropriate for the fault zone and the décollement. A numerical simulation was performed where rock conductivity is increased in the faults and décollement. Formation factor was chosen to be equal to 6 in order to induce a rock conductivity of 0.88 S/m within the faults and 0.70 S/m within the décollement, compared to 0.80 and 0.48 S/m in the sediments above and below reflector A, respectively. The hydraulic results are not dependent on the formation factor since the formation factor is not included in the pressure and fluid flow computation (equations (5), (6), and (7)). The electric potential remains the same as in Plate 3, since both the electric convection current and conduction current are proportional to the formation factor (the inverse of G in equation (8) and (9)) but opposite in direction, so that the important parameter for the electric potential distribution is the water conductivity (see equation (9)). However, since the electric current density is changed, the magnetic field is changed (see equation (10)), so that it is decreased by about a factor 3 (Plates 5a and 5b).

Let us now test the effect of the décollement width on the results of the numerical model. The décollement width could be lower, for example, 20 m, and it might affect the electric

potential and magnetic field results. A numerical simulation was performed with a décollement width of 20 m (Plate 6). In order to have reasonable overpressure (correct λ values between 0.7 and 0.9 in the décollement) in the faults zone the fluid velocity entering the décollement has been decreased, and the pressure gradient in the faults is decreased. The fluid velocity at the output of the thrust is decreased up to 0.2 m/yr for the second fault. In consequence, the electric potential is decreased by a factor 2 to 4, specially below the reflector A (Figure 5, solid symbols), the shape of the isovalues being the same, since the electric potential reflects directly the pressure field (equation (9)). The vertical electric field is 8.9 and 9.7 mV/km in the first 500 m depth for profiles above the vent (Figure 5, solid squares) and between the first and second vent (Figure 5, solid triangles). Below reflector A the vertical electric field is 48 to 52 mV/km (solid symbols, Figure 5). The horizontal gradient of the magnetic field remains about 2 nT/km, and the magnetic field is decreased by a factor 2 at the seafloor (Figure 6, solid symbols) and in depth (Figure 6): 4 and 5 nT/km for profiles above the vent (solid squares) and between the first and second vent (solid triangles), meaning that the total electric current density in the faults is decreased.

5. Discussion

When considering the first case of the simple analytical model where the electric current density is maximum within the faults

(equal to the convection current) and all the conduction current is within the sediments, we know that the magnetic field is inversely proportional to the formation factor (see equation (4')), so that a decrease in the formation factor (from 17 to 6, as performed when considering an increase in rock conductivity within the faults) would induce an increase in the magnetic field. On the contrary, when all the conduction current is confined within the faults, the total electric current density within the fault is zero and no magnetic field is induced (see section 3.1). Therefore the results of the numerical modeling, showing that the magnetic field is reduced when the rock conductivity of the faults and décollement are increased, mean that the back conduction current is reduced within the sediments and increased within the faults and the décollement. The reducing of contribution of the faults, it is why the isovalues of the magnetic field have not exactly the same shape (Plates 5a and 5b compared to Plates 4a and 4b).

5.1. In Situ Measurements of Fluid Flow Variations

The results of the model permit discussion of the sensor geometry to best measure the two parameters that could potentially be followed to monitor fluid flow variations: the electric field and the magnetic field, assuming steadystate flow. If boreholes were drilled into the accretionary prism, the vertical electric field could be measured between the levels in the borehole and the seafloor. Since the rate of potential increase with depth is larger when doing a profile between two vents than above one vent, it would be more appropriate to perform measurements between two vents. In that case the expected values of the potential deduced from Figure 5 (solid symbols, when the conductivity is high ($F=6$) in the décollement and in faults and the décollement width is 20 m) are -4, -9.5, -14.5, and -25 mV at depths of 200, 400, 600, and 800 m, respectively. The deeper the borehole, the larger the measured electric field. It is shown here that with the chosen geometry and when the back current is taken into account, the electric field has to be measured in boreholes instead of at the seafloor as proposed by Segawa and Toh [1992], who found an horizontal electric field of $\sim 1 \mu\text{V/m}$.

A measurement of the magnetic field implies borehole measurement or seafloor measurement in the faults domain. For the borehole measurements, as for the electric measurements, it would be more appropriate to drill between two vents since the rate of increase of the magnetic field is larger there (Figure 6). A differential measurement performed between the seafloor and levels in the borehole, when the conductivity is high ($F=6$) in the décollement and in faults and the décollement width is 20 m, could yield a magnetic field intensity of 5.5, 6.5, 7.5, and 8.5 nT at depths of 200, 400, 600, and 800 m, respectively. The deeper the borehole, the larger the measured magnetic field.

Note that all the measurements could be performed in the same borehole drilled between two vents since it seems more appropriate for both electric and magnetic fields. Monitoring fluid flow variations implies the ability to follow the temporal variations of the electric and magnetic field.

5.2. Temporal Variations

Fluid inclusion analysis on rocks from the Kodiak accretionary complex showed that fluid pressures drop by 20% to 45% during the growth of quartz veins, suggesting that the deformation induces a local effect of fluid escaping to shallow levels in the subduction complex, possibly along an

interconnected fracture network [Vrolijk, 1987]. The model proposed by Vrolijk implies cyclic variations of fluid pressure at near-lithostatic pressure. Moore [1989] proposed that episodicity of fluid flow along décollement zones may be explained by a deformational pumping mechanism by cycles of dilatation and flow to the décollement zone followed by failure and fluid expulsion along the décollement zone. Moreover, calculations based on thermal gradient and heat flow data from the Barbados accretionary complex are consistent with transient fluid flow along high-permeability conduits within the sediments, starting and stopping over intervals of decade to tens of thousands of years [Fisher and Hounslow, 1990]. At a shorter scale > 1 month, on the Nankai accretionary wedge, Darcy velocity deduced from temperature measurements to a depth of 60 cm over a very active fluid vent (fluid velocity of 100 m/yr) has shown fluctuations of $\sim 15\%$ which may be periodic and has shown an increase of 30% over the 1 month period of the observation [Foucher et al., 1992]. We therefore consider a change of 20% in the fluid flow velocity due to a 20% change in the fluid pressure. The resulting variations in the streaming potential and magnetic field inside a borehole between two vents, when the conductivity is high ($F=6$) in the décollement and in faults and the décollement width is 20 m, are expected to be -1.9 mV and 1.3 nT at depth 400 m, -2.9 mV and 1.5 nT at depth 600 m, and -5 mV and 1.7 nT at depth 800 m. Direct fluid pressure measurements could be performed in borehole to complete these electric measurements. When monitoring the magnetic field at the seafloor, the variation is expected to be a change of 0.4 nT/km. Since the streaming potential is proportional to the fluid pressure, this justifies the use of a steadystate model in describing such variations of fluid pressure, streaming potential, and magnetic field anomaly. Note that if the fluid velocity change is only due to a permeability change (pressure gradient constant), then the streaming potential will remain constant (see equation (8)).

What about possible coupled change in permeability, fluid velocity, and fluid pressure? The permeability along the décollement is presumably much lower when pore pressure is low and fluid is not allowed to flow [Fisher and Hounslow, 1990]. High permeabilities are thought to be associated with anomalously high fluid pressures and fluid flow as implied by geochemical and thermal anomalies correlated with the décollement zone [Gieskes et al., 1990; Kastner et al., 1993]. Rhodochrosite filled veins in the scaly fabrics of the décollement zone at the Barbados ridge suggest that fluid pressures were sufficiently high to allow the décollement zone to open for fluid flow [Moore et al., 1987]. If an increase in permeability and in pressure occurs in the décollement and in the major thrusts, the streaming potential will be increased, but only by the amount of the pressure increase as shown by equation (9).

Fluid flow can be deduced from pressure gradient measurements within venting clam colonies. In that case, some difficulties in inserting the probes into indurated sediments may arise [Le Pichon et al., 1992]. Fluid flow can also be deduced from temperature measurements; however, only Darcian velocities > 10 m/yr can be reasonably estimated. Moreover, fluctuations in the bottomwater temperature may perturb the measurements. For example, data collected during the Kaiko-Nankai cruise at 2000 m depth were impossible to use because of a temperature variation at the bottom water of 1°C [Henry et al., 1992].

The method that we propose to detect fluid circulation changes is therefore to monitor the vertical electric field and the

horizontal magnetic field in a borehole and the magnetic field at the seafloor near the source. Since changes of fluid circulation that may be related to seismic activity are expected to have a long timescale variation, we need to monitor the electric field during several years with the technical problems that are implied. To measure the electric field, the electrodes must be very stable with time [Filloux, 1987; Petiau and Dupis, 1980; Perrier et al., 1997]. In order to perform measurements in wells the boreholes must produce minimum perturbation of fluid circulation and in electric current paths. Therefore the use of the steel casing is not possible, and the use of an openhole causes the tools to be lost in the hole collapse.

The variations of the magnetic field are measurable, considering that a installed nuclear magnetic resonance (nmr) magnetometer has an accuracy of 0.05-0.1 nT with an appropriate reference for differential measurements. These nmr magnetometers measure the modulus of the magnetic field, i.e., the projection of the anomaly in the direction of the Earth's magnetic field to a first-order approximation. Note that the measurements at the seafloor are likely to be disturbed by the water movement at all scales from local bottom currents to large-scale oceanic streams as the "Kuroshio" western boundary ocean current [Segawa and Toh, 1992].

6. Conclusion

We showed that the fluid circulation in an accretionary prism could produce an electric field and a magnetic field due to electrokinetic coupling. The detection of fluid flow rate variations could be best performed by monitoring the vertical electric field and the vertical gradient of the horizontal magnetic field in a borehole drilled between two vents and by monitoring the horizontal gradient of the magnetic field at the seafloor. A variation of 3 mV and 1.5 to 3 nT at 600 m depth in a borehole could reveal a fluid flow rate variation of 20%, which is a reasonable fluid flow change based on some observations at short-scale time. Since a 1.5 to 3 nT anomaly seems easier to detect than a 3 mV anomaly, it is likely that the variation of the magnetic field would more sensitively reveal fluid flow variations. When monitoring the magnetic field at the seafloor, a change of 0.4 nT/km in the horizontal gradient could reveal a fluid flow rate variation of 20%.

Acknowledgments. We thank Pierre Henry for his highly fruitful conversations. The review of the manuscript by H. J. Tobin and two anonymous reviewers greatly improved the constraints of the model and the discussion. This research was supported by CNRS-INSU. This is CNRS-INSU-DBT contribution 161 thème fluides et failles, CNRS-INSU-PNRN contribution 159 thème risques sismiques, and CNRS-INSU-PNRH contribution 160 thème circulation des fluides dans la croûte.

References

- Boulègue, J., X. Le Pichon, and J.T. Iiyama, Earthquake prediction in Tokai area (Japan), *C. R. Acad. Sci. Paris, Sér. II*, 301, 1217-1219, 1985.
- Cloos, M., Landward-dipping reflectors in accretionary wedges: Active dewatering conduits?, *Geology*, 12, 519-522, 1984.
- Davis, D., J. Suppe, and F.A. Dahlen, Mechanics of fold-and-thrust belts and accretionary wedges, *J. Geophys. Res.*, 88, 1153-1172, 1983.
- Dukhin, S.S., and B.V. Derjaguin, *Surface and Colloid Science*, vol. 7, *Electrokinetic Phenomena*, edited by E. Matijevic, John Wiley, New York, 1974.
- Durand, E., *Electrostatique et Magnéto-statique*, pp. 499, Masson, Paris, 1953.
- Filloux, J.H., Instrumentation and experimental methods for oceanic studies, in *Geomagnetism*, vol. 1, edited by J. A. Jacobs, pp. 143-248, Academic, San Diego, Calif., 1987.
- Fisher, A.T., and M.W. Hounslow, Transient fluid flow through the toe of the Barbados accretionary complex: Constraints from Ocean Drilling Program Leg 110 heat flow studies and simple models, *J. Geophys. Res.*, 95, 8845-8858, 1990.
- Fitterman, D.V., Electrokinetic and magnetic anomalies associated with dilatant regions in a layered Earth, *J. Geophys. Res.*, 83, 5923-5928, 1978.
- Foucher, J.-P., P. Henry, X. Le Pichon, and K. Kobayashi, Time-variations of fluid expulsion velocities at the toe of the eastern Nankai accretionary complex, *Earth Planet. Sci. Lett.*, 109, 373-382, 1992.
- Gieskes, J.M., G. Bland, P. Vrolijk, H. Elderfield, and R. Barnes, Interstitial water chemistry-major constituents, in *Proc. Ocean Drill. Program Sci. Results, Part B*, 110, 155-178, 1990.
- Gieskes, J.M., T. Gamo, and M. Kastner, Major and minor element geochemistry of interstitial waters of site 808, Nankai Trough: An overview, in *Proc. Ocean Drill. Program, Sci. Results*, 131, 387-396, 1993.
- Heinson, G., and J. Segawa, Electrokinetic signature of the Nankai Trough accretionary complex: preliminary modelling for the Kaiko-Tokai program, *Phys. Earth Planet. Inter.*, 99, 33-53, 1997.
- Henry, P., and X. Le Pichon, Fluid flow along a décollement layer: A model applied to the 16°N section of the Barbados accretionary wedge, *J. Geophys. Res.*, 96, 6507-6528, 1991.
- Henry, P., J.-P. Foucher, X. Le Pichon, M. Sibuet, K. Kobayashi, P. Tarits, N. Chamot-Rooke, T. Furuta, and P. Schultheiss, Interpretation of temperature measurements from Kaiko-Nankai cruise: Modeling of fluid flow in clam colonies, *Earth Planet. Sci. Lett.*, 109, 355-371, 1992.
- Hubbert, M.K., and W.W. Rubey, Role of fluid pressure in mechanics of overthrust faulting, *Geol. Soc. Am. Bull.*, 70, 115-166, 1959.
- Hyndman, R.D., G.F. Moore, and K. Moran, Velocity, porosity and pore-fluid loss from the Nankai subduction zone accretionary prism, in *Proc. Ocean Drill. Program, Sci. Results*, 131, 211-220, 1993.
- Ishibashi K., Specification of soon-to-occur seismic faulting in the Tokai district, Central Japan, based upon seismotectonics, in *Earthquake Prediction: An International Review*, edited by D.W. Simpson and P.G. Richards, pp. 297-332, *Maurice Ewing Ser.*, vol. 4, Washington, D.C., 1981.
- Ishido, T., and H. Mizutani, Experimental and theoretical basis of electrokinetic phenomena in rock-water systems and its applications to geophysics, *J. Geophys. Res.*, 86, 1763-1775, 1981.
- Jouniaux, L., and J.-P. Pozzi, Streaming potential and permeability of saturated sandstones under triaxial stress: Consequences for electrotelluric anomalies prior to earthquakes, *J. Geophys. Res.*, 100, 10197-10209, 1995a.
- Jouniaux, L., and J.-P. Pozzi, Permeability dependence of streaming potential in rocks for various fluid conductivities, *Geophys. Res. Lett.*, 22, 485-488, 1995b.
- Jouniaux, L., and J.-P. Pozzi, Anomalous 0.1-0.5 Hz streaming potential measurements under geochemical changes: Consequences for electrotelluric precursors to earthquakes, *J. Geophys. Res.*, 102, 15335-15343, 1997.
- Jouniaux, L., S. Lallemand, and J.-P. Pozzi, Changes in the permeability, streaming potential and resistivity of a claystone from the Nankai prism under stress, *Geophys. Res. Lett.*, 21, 149-152, 1994.
- Jouniaux, L., M. Dubet, M. Zamora, and P. Morat, Physical properties of limestone from the quarry of Meriel, *C. R. Acad. Sci. Paris, Ser. IIA*, 322, 361-367, 1996.
- Kastner, M., H. Elderfield, W.J. Jenkins, J.M. Gieskes, and T. Gamo, Geochemical and isotopic evidence for fluid flow in the western Nankai subduction zone, Japan, in *Proc. Ocean Drill. Program, Sci. Results*, 131, 397-413, 1993.
- Langseth, M.G., and J.C. Moore, Introduction to special section on the role of fluids in sediment accretion, deformation, diagenesis, and metamorphism in subduction zones, *J. Geophys. Res.*, 95, 8737-8741, 1990.
- Le Pichon, X., K. Kobayashi, and Kaiko-Nankai Scientific Crew, Fluid venting activity within the eastern Nankai Trough accretionary wedge: A summary of the 1989 Kaiko-Nankai results, *Earth Planet. Sci. Lett.*, 109, 303-318, 1992.
- Lorne, B., F. Perrier, and J.-P. Avouac, Streaming potential measurements: 1. Properties of the electrical double layer from crushed rock samples, *J. Geophys. Res.*, 104, 17857-17877, 1999a.
- Lorne, B., F. Perrier, and J.-P. Avouac, Streaming potential measurements: 2. Relationship between electrical and hydraulic flow

- patterns from rock samples during deformation, *J. Geophys. Res.*, **104**, 17879-17896, 1999b.
- Massé, P., and J. Berthier, Three dimensional finite element modelling of streaming potential and associated magnetic field in porous media, paper presented at *Conference on the Computation of Electromagnetic Fields (COMPUMAG)*, Berlin, July 10-13, 1995.
- Massé, P., and J. Berthier, Three dimensional finite element modeling of streaming potential and associated magnetic field, *Trans. Magn.*, **32**, 994-998, 1996.
- Moore, G.F., T.H. Shipley, P.L. Stoffa, D.E. Karig, A. Taira, S. Kuramoto, H. Tokuyama, and K. Suyehiro, Structure of the Nankai Trough accretionary zone from multichannel seismic reflection data, *J. Geophys. Res.*, **95**, 8753-8765, 1990.
- Moore, J.C., Tectonics and hydrogeology of accretionary prisms: Role of the décollement zone, *J. Struct. Geol.*, **11**, 95-106, 1989.
- Moore, J.C., and P. Vrolijk, Fluids in accretionary prisms, *Revi. Geophys.*, **30**, 113-135, 1992.
- Moore, J.C., and ODP Leg 110 Scientific party, Expulsion of fluids from depth along a subduction-zone décollement horizon, *Nature*, **326**, 785-788, 1987.
- Moore, J.C., et al., Tectonics and hydrogeology of the northern Barbados Ridge: Results from Ocean Drilling Program Leg 110, *Geol. Soc. Am. Bull.*, **100**, 1578-1593, 1988.
- Moran, K., W. Brückmann, V. Feeser, and R.G. Campanella, In-situ stress conditions at Nankai Trough, site 808, in *Proc. Ocean Drill. Project, Sci. Results*, **131**, 283-291, 1993.
- Morgan, J.K., and D.E. Karig, Décollement processes at the Nankai accretionary margin, southeast Japan: Propagation, deformation, and dewatering, *J. Geophys. Res.*, **100**, 15221-15231, 1995.
- Nourbehecht, B., Irreversible thermodynamic effects in inhomogeneous media and their applications in certain geoelectric problems, Ph.D. thesis, Mass. Inst. of Technol., Cambridge, 1963.
- Overbeek, J.T., Electrochemistry of the double layer, in *Colloid Science*, vol. I, *Irreversible Systems*, edited by H. R. Kruyt, pp. 115-193, Elsevier, New York, 1952.
- Perrier, F., et al., A one year systematic study of electrodes for long period measurements of the electric field in geophysical environments, *J. Geomagnet. Geoelectr.*, **49**, 1677-1696, 1997.
- Petiau, G., and A. Dupis, Noise, temperature coefficient, and long time stability of electrodes for telluric observations, *Geophys. Prospect.*, **28**, 792-804, 1980.
- Poirier, J.E., and J.M. Cases, Sur l'origine et la nature de l'interaction adsorbant-adsorbant dans les systèmes à interactions faibles, in *Solid-Liquid Interactions in Porous Media*, pp. 447-462, Technip, Colloque Bilan, Nancy, France, 1985.
- Pride, S.R., and F.D. Morgan, Electrokinetic dissipation induced by seismic waves, *Geophysics*, **56**, 914-925, 1991.
- Revil, A., and P.W.J. Glover, Theory of ionic-surface electrical conduction in porous media, *Phys. Rev. B*, **55**, 1757-1773, 1997.
- Screaton, E.J., D.R. Wuthrich, and S.J. Dreiss, Permeabilities fluid pressure and flow rates in the Barbados ridge complex, *J. Geophys. Res.*, **95**, 8997-9007, 1990.
- Segawa, J., and H. Toh, Detecting fluid circulation by electric field variations at the Nankai Trough, *Earth Planet. Sci. Lett.*, **109**, 469-476, 1992.
- Sharma, M.M., J.F. Kuo, and T.F. Yen, Further investigation of the surface charge properties of oxide surfaces in oil-bearing sands and sandstones, *J. Colloid Interface Sci.*, **115**, 9-16, 1987.
- Sibson, R. H., J.M. Moore, and A.H. Rankin, Seismic pumping-a hydrothermal fluid transport mechanism, *J. Geol. Soc. London*, **131**, 653-659, 1975.
- Somasundaran, P., and R.D. Kulkarni, A new streaming apparatus and study of temperature effects using it, *J. Colloid Interface Sci.*, **45**, 591-600, 1973.
- Stern, O., Zur theorie der elektrolytischen doppelschicht, *Z. Elektrochem.*, **30**, 508, 1924.
- Taira, A., et al., Geological background and objectives, by shipboard scientific party, in *Proc. Ocean Drill. Program, Initial Rep.*, **131**, 5-14, 1991.
- Taira, A., et al., Proceedings of the Ocean Drilling Initial Reports, vol. 131, site 808, p. 213, Ocean Drill. Program, College Station, Tex., 1990.
- Taylor, E., and A. Fisher, Sediment permeability at the Nankai accretionary prism, site 808, in *Proc. Ocean Drill. Program, Sci. Results*, **131**, 235-243, 1993.
- von Huene, R., and H. Lee, The possible significance of pore fluid pressure in subductions zones, edited by J.S. Watkins, and C.L. Drake, *Stud. Cont. Margin Geol.*, **34**, 781-791, 1982.
- Vrolijk, P., Tectonically driven fluid flow in the Kodiak accretionary complex, Alaska, *Geology*, **15**, 466-469, 1987.
- Westbrook, G.K., and M.J. Smith, Long décollements and mud volcanoes: Evidence from the Barbados ridge complex for the role of high pore-fluid pressure in the development of an accretionary complex, *Geology*, **11**, 279-283, 1983.
- Westbrook, G.K., M.J. Smith, J.H. Peacock, and M.J. Poulter, Extensive underthrusting of underformed sediment beneath the accretionary complex of the Lesser Antilles subduction zone, *Nature*, **300**, 625-628, 1982.
- Winkler, W.R., and N.J. Steward, Proceedings of the Ocean Drilling Program Scientific Results, vol. 131, site 808, Ocean Drill. Program, College Station, Tex., 1991.

J. Berthier, and P. Massé, LETI (CEA-Technologies avancées) DSYS, CEA Grenoble, 17 rue des Martyrs, 38054 Grenoble Cédex 9, France. (jberthier@cea.fr)

L. Jouniaux, and J.-P. Pozzi, Laboratoire de Géologie & CNRS UMR 8538, École Normale Supérieure, 24 rue Lhomond, 75231 Paris Cedex 05, France. (jouniaux@magnetit.ens.fr; pozzi@magnetit.ens.fr)

(Received June 8, 1998; revised March 10, 1999; accepted March 11, 1999.)